Electronic Supplementary Material (ESI) for Nanoscale.
This journal is © The Royal Society of Chemistry 2022

Supporting Information: Two-dimensional Ferroelectric MoS_2/Ga_2O_3 Heterogeneous Bilayers with Highly Tunable Photocatalytic and Electrical Properties

Haohao Chen[∇,†] Junlei Zhao[∇,†] Xinyu Wang,[†] Xiaolong Chen,[†] Zhaofu Zhang,[*,‡] and Mengyuan Hua[*,†]

†*Department of Electrical and Electronic Engineering, Southern University of Science and Technology, Shenzhen 518055, China*

‡*Department of Engineering, University of Cambridge, Cambridge CB2 1PZ, United Kingdom*

E-mail: zz389@cam.ac.uk; huamy@sustech.edu.cn

Extended Computational data

Searching of Stable Stacking Configurations

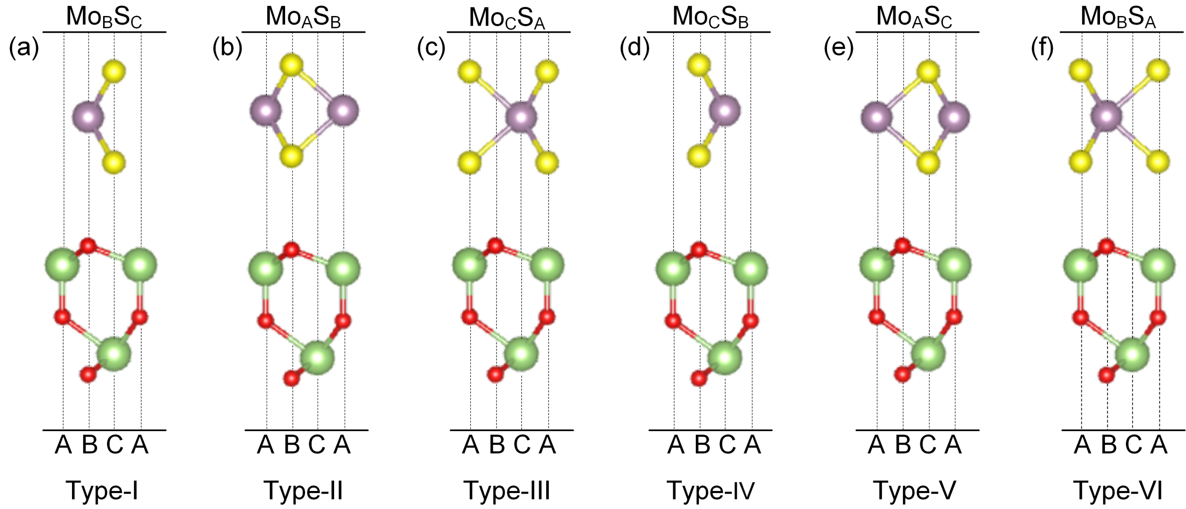

Fig. S1 Schematic views of relaxed $MoS_2/Ga_2O_3\uparrow$ heterostructures with various high-symmetry atomic arrangements. (a) to (f) are labeled as Type-I to Type-VI, respectively.

Table S1: Energy difference of $MoS_2/Ga_2O_3\uparrow$

Heterostructure	Energy Difference (meV per unit cell)
Type-I	6.55
Type-II	61.07
Type-III	0
Type-IV	60.44
Type-V	5.93
Type-VI	2.78

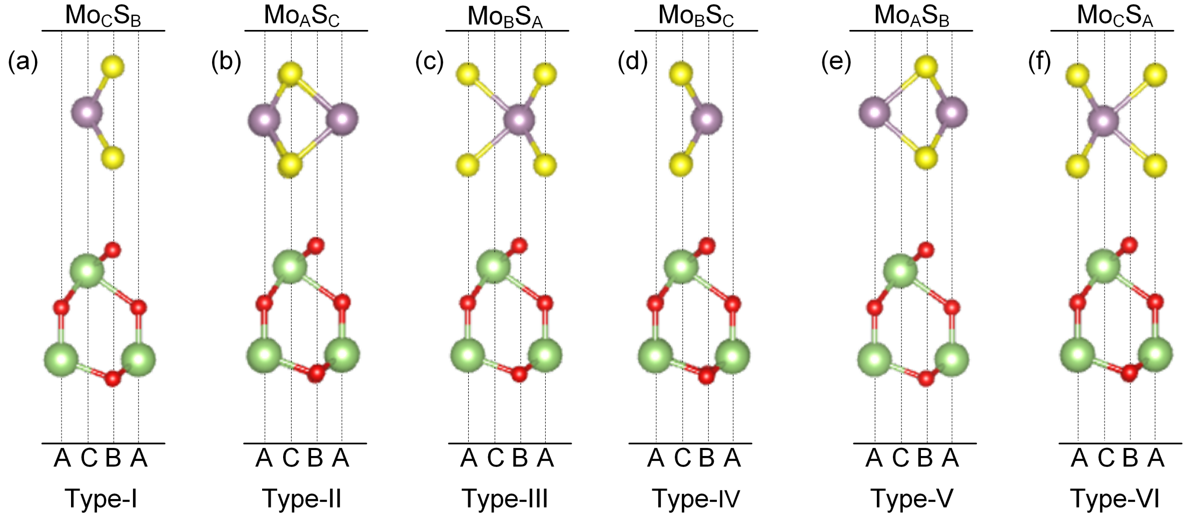

Fig. S2 Schematic views of relaxed $MoS_2/Ga_2O_3\downarrow$ heterostructures with various high-symmetry atomic arrangements. (a) to (f) are labeled as Type-I to Type-VI, respectively.

Table S2: Energy difference of $MoS_2/Ga_2O_3\downarrow$

Heterostructure	Energy Difference (meV per unit cell)
Type-I	64.27
Type-II	1.81
Type-III	4.04
Type-IV	5.39
Type-V	64.20
Type-VI	0

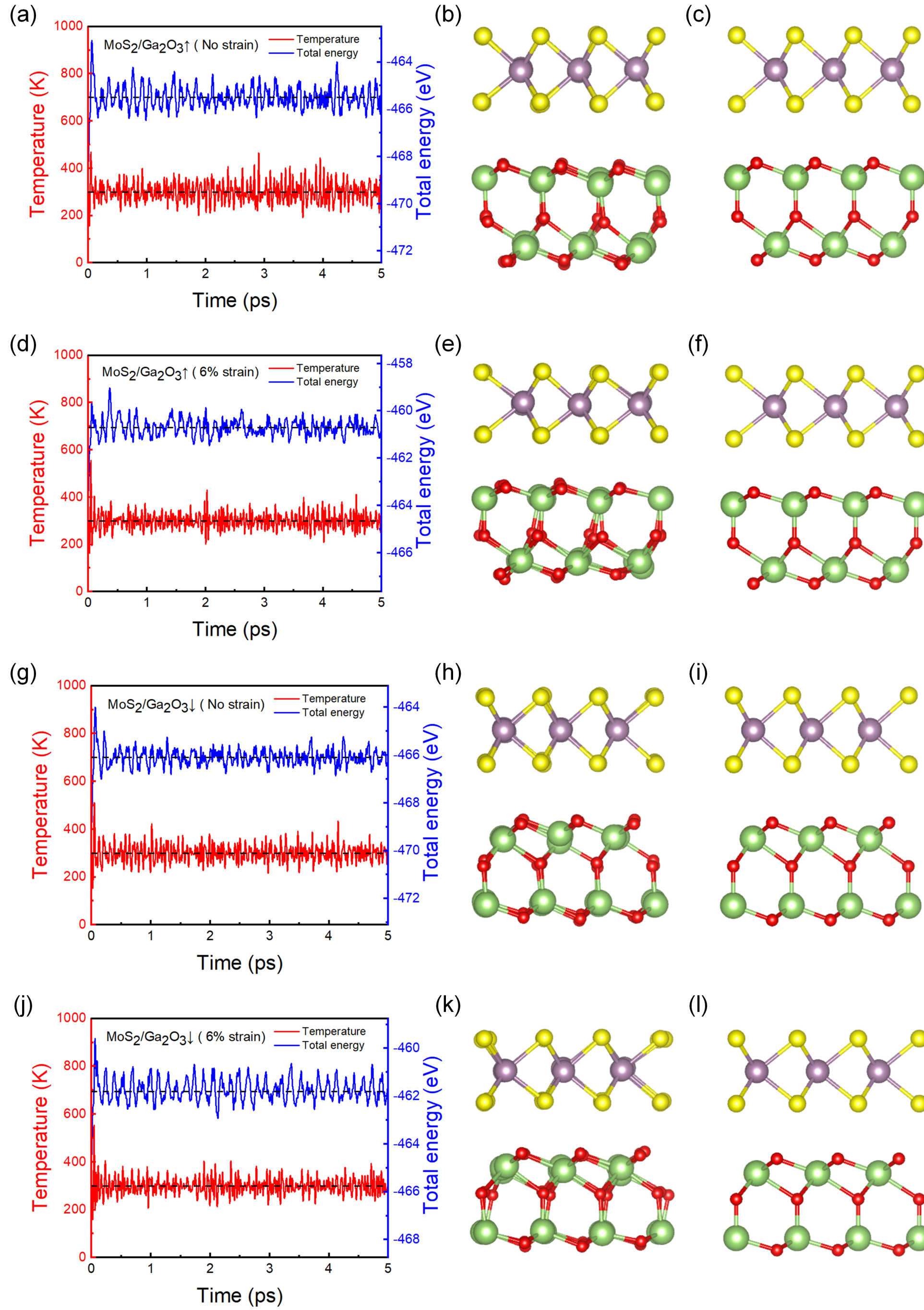

Fig. S3 Evolution of temperature (red, left axis) and total energy (blue, right axis) with time during AIMD simulations for (a, d) $MoS_2/Ga_2O_3\uparrow$ and (g, j) $MoS_2/Ga_2O_3\downarrow$ heterostructures under relaxed station and 6% tensile strain, respectively. Atomic structures of the heterostructures after (b,e,h,k) 5 ps AIMD simulations at 300 K and further (c,f,i,l) geometry relaxations, respectively.

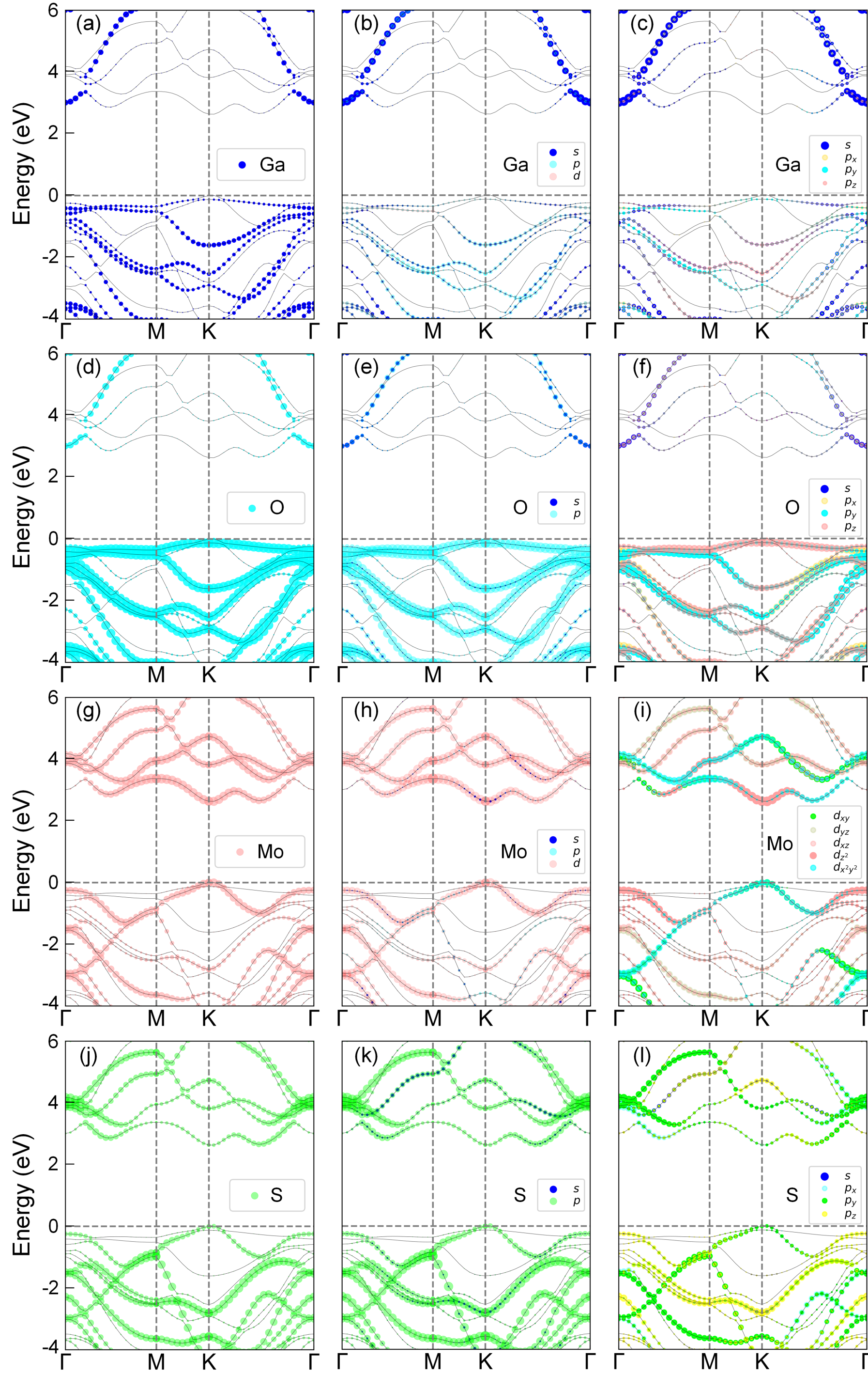

Fig. S4 Projected band structure of $MoS_2/Ga_2O_3\uparrow$ heterostructure for orbitals of (a) Ga (b) Ga-s, Ga-p, Ga-d (c) Ga-s, Ga-p_x, Ga-p_y, Ga-p_z (d) O (e) O-s, O-p (f) O-s, O-p_x, O-p_y, O-p_z (g) Mo (h) Mo-s, Mo-p, Mo-d (i) Mo-d_{xy}, Mo-d_{yz}, Mo-d_{xz}, Mo-d_{z^2}, Mo-$d_{x^2-y^2}$ (j) S (k) S-s, S-p (l) S-s, S-p_x, S-p_y, S-p_z, respectively.

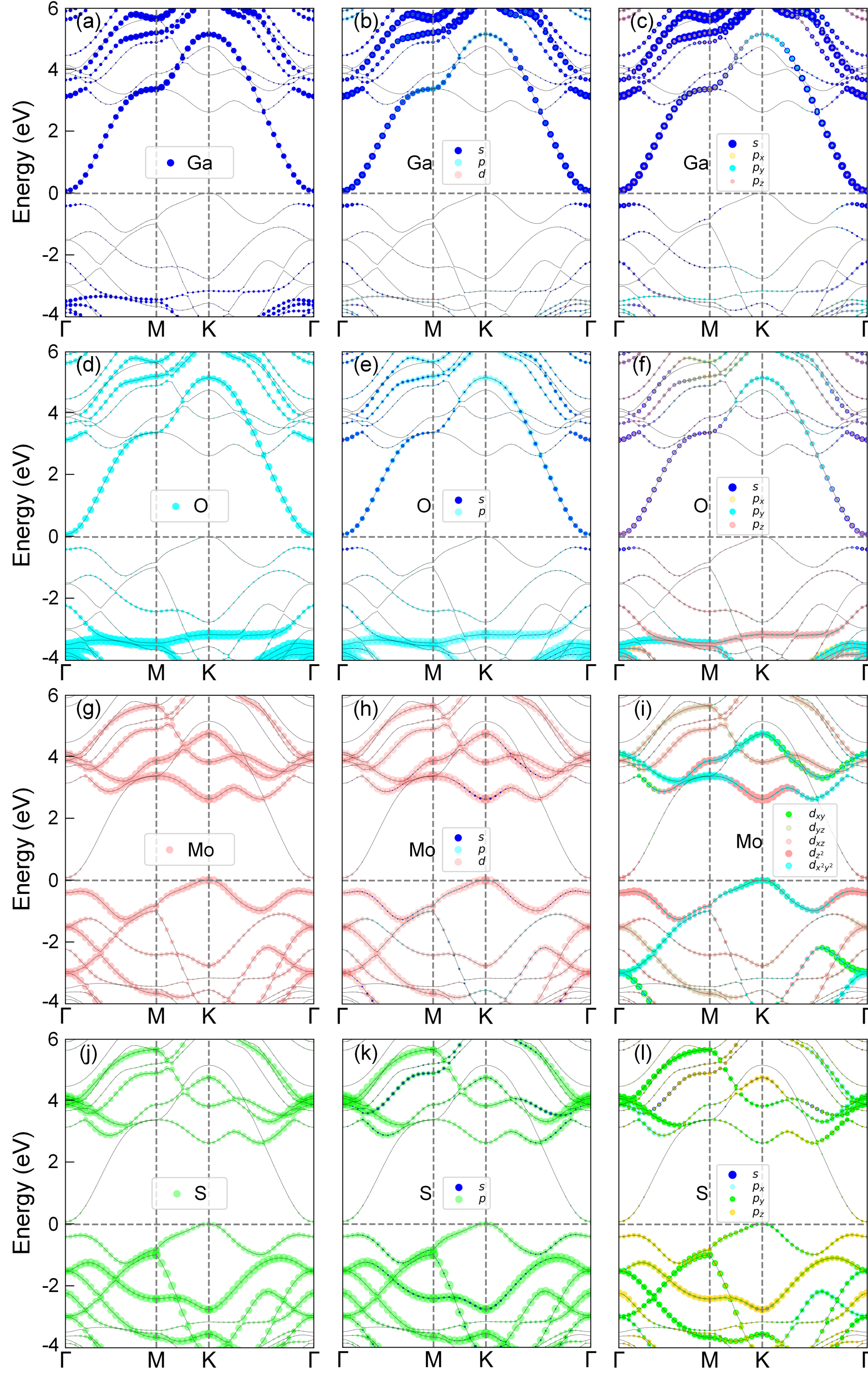

Fig. S5 Projected band structure of MoS_2/Ga_2O_3↓ heterostructure for orbitals of (a) Ga (b) Ga-s, Ga-p, Ga-d (c) Ga-s, Ga-p_x, Ga-p_y, Ga-p_z (d) O (e) O-s, O-p (f) O-s, O-p_x, O-p_y, O-p_z (g) Mo (h) Mo-s, Mo-p, Mo-d (i) Mo-d_{xy}, Mo-d_{yz}, Mo-d_{xz}, Mo-d_{z^2}, Mo-$d_{x^2-y^2}$ (j) S (k) S-s, S-p (l) S-s, S-p_x, S-p_y, S-p_z, respectively.

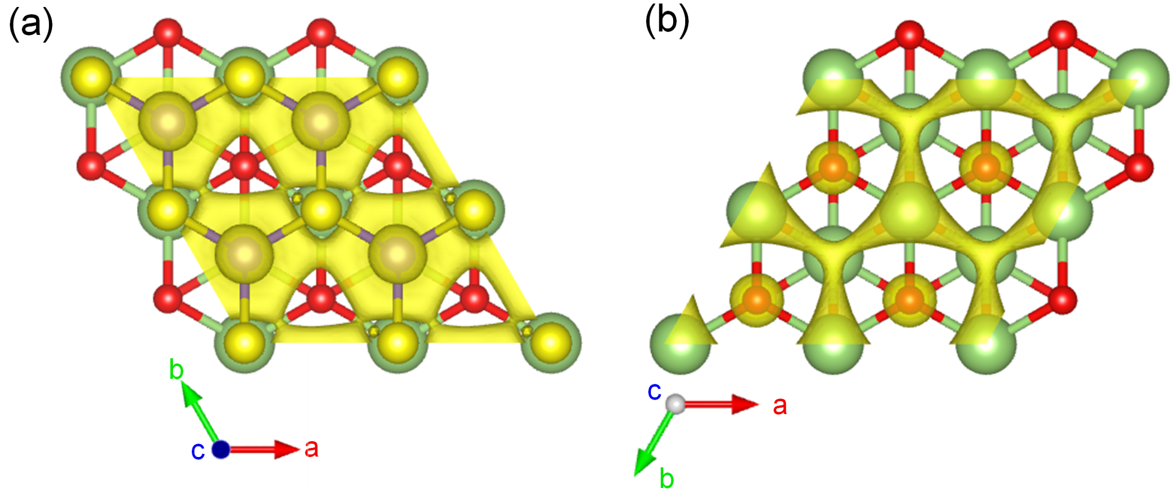

Fig. S6 Partial real-space probability distribution at CBM of (a) $MoS_2/Ga_2O_3\uparrow$ and (b) $MoS_2/Ga_2O_3\downarrow$, with the same isosurface level at 3.21 $\times 10^{-8}$ e/Bohr^3.

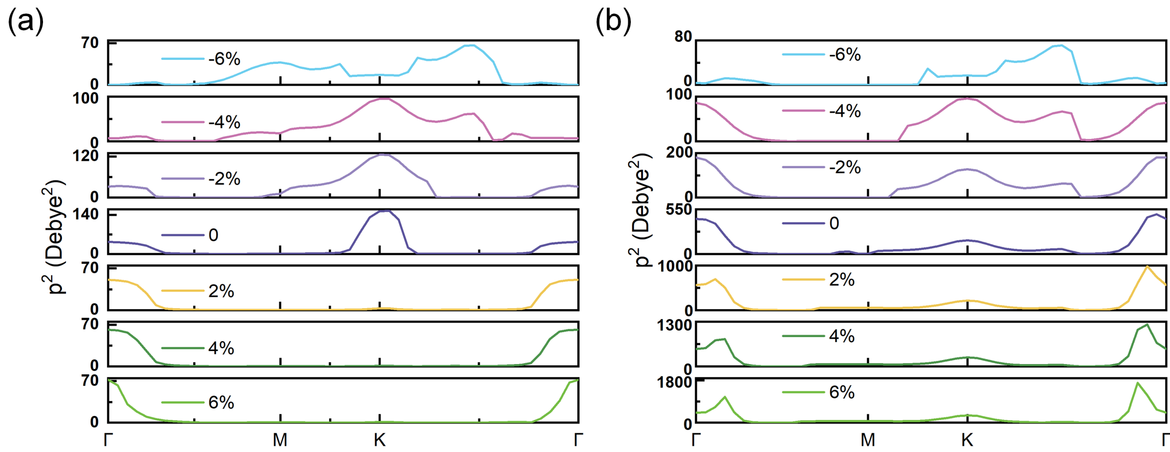

Fig. S7 Transition dipole moment of (a) $MoS_2/Ga_2O_3\uparrow$ and (b) $MoS_2/Ga_2O_3\downarrow$ versus biaxial strains.

The squared transition dipole moment (P^2) between the highest valence band and the lowest conduction band can be used to represent the transition probability of electrons,[S1,S2] as shown in Fig. S7a,b.

For $MoS_2/Ga_2O_3\uparrow$, with decreasing compressive strain and increasing tensile strain, the transition probability of electrons tends to increase in the Γ point region. In the high-symmetry K point region, the electron transition probability under tensile strain is much

smaller than that of compressive strain. This is because under tensile strain conditions, the conduction band is derived from MoS_2, while the valance band is occupied by Ga_2O_3. The electronic transition not only overcomes the band gap but also considers the effect of interlayer transition and intrinsic dipole moment on electrons. It is obvious that P^2 of $MoS_2/Ga_2O_3\downarrow$ is much higher than $MoS_2/Ga_2O_3\uparrow$. What's more, under the tensile strain of 6%, the electron transition with three-times enhancement in $MoS_2/Ga_2O_3\downarrow$ is observed due to gap narrowing near the Γ region. As a result, the high P^2 and good light absorption show advantages and potentials in solar energy conversion such as photocatalytic water splitting and photodetection.

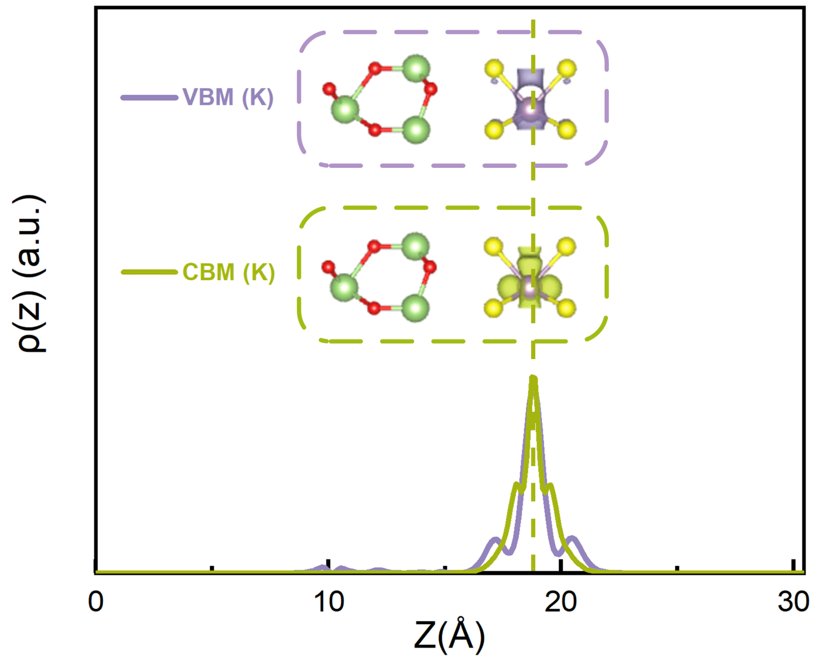

Fig. S8 The real-space probability distribution of $MoS_2/Ga_2O_3\uparrow$ heterostructure along the z direction. The insets show its real-space probability distribution of VBM (K) and CBM (K), respectively, with the same isosurface level at 3.21 $\times 10^{-8}$ e/Bohr^3.

References

(S1) Meng, W.; Wang, X.; Xiao, Z.; Wang, J.; Mitzi, D. B.; Yan, Y. Parity-forbidden transitions and their impact on the optical absorption properties of lead-free metal halide perovskites and double perovskites. *J. Phys. Chem. Lett.* **2017**, *8*, 2999–3007.

(S2) Liao, Y.; Zhang, Z.; Gao, Z.; Qian, Q.; Hua, M. Tunable properties of novel Ga_2O_3 monolayer for electronic and optoelectronic applications. *ACS Appl. Mater. Interfaces* **2020**, *12*, 30659–30669.